

Solvation enhances folding cooperativity and the topology dependence of folding rates in a lattice protein model

Nhung T. T. Nguyen,^{1,2} Pham Nam Phong,³ Duy Manh Le,^{4,5} Minh-Tien Tran,² and Trinh Xuan Hoang^{2, a)}

¹⁾ *Graduate University of Science and Technology, Vietnamese Academy of Science and Technology, 18 Hoang Quoc Viet, Nghia Do, Cau Giay, Hanoi 11307, Vietnam*

²⁾ *Institute of Physics, Vietnamese Academy of Science and Technology, 10 Dao Tan, Ba Dinh, Hanoi 11108, Vietnam*

³⁾ *Faculty of Engineering Physics, Hanoi University of Science and Technology, 1 Dai Co Viet Road, Hanoi, Vietnam*

⁴⁾ *Laboratory of Advanced Materials and Natural Resources, Institute for Advanced Study in Technology, Ton Duc Thang University, Ho Chi Minh City, Vietnam*

⁵⁾ *Faculty of Applied Sciences, Ton Duc Thang University, Ho Chi Minh City, Vietnam*

The aqueous solvent profoundly influences protein folding, yet its effects are relatively poorly understood. In this study, we investigate the impact of solvation on the folding of lattice proteins by using Monte Carlo simulations. The proteins are modelled as self-avoiding 27-mer chains on a cubic lattice, with compact native states and structure-based Gō potentials. Each residue that makes no contacts with other residues in a given protein conformation is assigned a solvation energy ε_s , representing its full exposure to the solvent. We find that a negative ε_s , indicating a favorable solvation, increases the cooperativity of the folding transition by lowering the free energy of the unfolded state, increasing the folding free energy barrier, and narrowing the folding routes. This favorable solvation also significantly improves the correlation between folding rates and the native topology, measured by the relative contact order. Our results suggest that Gō model may overestimate the importance of native interactions and a solvation potential countering the native bias can play a significant role. The solvation energy in our model can be related to the polar interaction between water and peptide groups in the protein backbone. It is therefore suggested that the solvation of peptide groups may significantly contribute to the exceptional folding cooperativity and the pronounced topology-dependence of folding rates observed in two-state proteins.

I. INTRODUCTION

Water plays a fundamental role in protein folding, mainly through the dominance of the hydrophobic effect^{1–3} in the folding and stabilization of proteins. Water also influences helix propensities of amino acids⁴ and regulates protein aggregation⁵. The extent of water-mediated effects on protein folding remains elusive, despite extensive research. It has been shown experimentally that solvation free energies are pairwise non-additive⁶, complicating the modeling and analysis of proteins by requiring many-body interactions⁷. The particulate nature of water gives rise to a desolvation barrier^{8–10} to hydrophobic cluster formation, which may contribute to the rate-limiting step in protein folding^{11–13}. The role of solvents extends beyond water, as changes in the solvent conditions such as pH, ionic strength, or the presence of denaturants, can modulate the folding rates and outcomes¹⁴. Simulating folding kinetics at atomic resolution, whether with explicit or implicit solvents, remains highly computationally demanding^{15,16}. Meanwhile, valuable insights into the role of solvents on protein folding can be obtained using simple lattice^{17,18}, off-lattice^{11–13} and continuous^{19,20} models.

In this study, we examine the role of solvation in deter-

mining two remarkable properties of two-state proteins—a class of small, single-domain proteins that fold essentially with simple two-state kinetics^{21,22}. One is folding cooperativity, which refers to the ability of proteins to exhibit a sharp transition between the unfolded and folded states without significant intermediate states, resembling an “all-or-none” process²³. Two-state proteins exhibit surprisingly high folding cooperativity in both kinetic and thermodynamic aspects, compared to those obtained from simulations^{24–26}. The other property is the topology dependence of folding rates, an important observation made by Plaxco et al.^{27,28}. These authors discovered a strong correlation between the logarithms of experimentally observed folding rates for two-state proteins and the relative contact order²⁷, which is defined as the average sequence separation of native contacts relative to the protein chain length. This empirical result called into question early theories and simulations regarding the folding rates, many of which suggested that chain length is a dominant factor^{29–34}. Despite significant progress^{35–50}, our understanding of the physical basis for the rate-topology dependence remains limited. It was suggested that the rate-topology dependence is a consequence of the extraordinary folding cooperativity in two-state proteins⁴¹. Thus, our goal is to check if solvation contributes to the folding cooperativity and whether its increase is associated with the increase in the rate-topology dependence.

Gō⁵¹ and Gō-like models^{52–54} have been widely used

^{a)}Corresponding author, Email: txhoang@iop.vast.vn

for studying the folding mechanism^{55,56}, offering insights into how the folding process is driven solely by native interactions. Despite this global native preference, these models show moderate folding cooperativity^{23–25} and insignificant to low correlations between folding rates and the relative contact order^{48–50}. Jewett et al.⁴¹ demonstrated that adding an explicit energetically cooperative feature to the Hamiltonian of the lattice Gō model can give rise to the rate-topology correlation. Another modification to the Gō model that leads to a similar effect was given by Kaya and Chan⁴², who introduced a coupling between non-local contact interactions and local conformational preferences. These studies indicate that an energetic component leading to folding cooperativity is missing in the Gō model. More recently, by using an off-lattice Gō-like model with desolvation barriers in the pairwise potentials, Chan and coworkers^{44–47} showed that the desolvation barriers can substantially enhance folding cooperativity and the diversity in the folding rates, while their impact on the rate-topology correlation is modest.

Here, we propose a modification to the Gō model by incorporating a solvation energy term that favors fully solvent-exposed residues. This modification is based on a hypothesis that Gō potentials may overemphasize the contributions of native interactions to folding free energy, thereby undermining favorable solvent-protein interactions in the unfolded state, such as the polar interaction between water and exposed peptide groups in an unfolded protein. Not only competing with native interactions, the proposed solvation energy can also energetically disfavor the formation of non-native contacts. Finally, the solvation energy term represents a many-body interaction, enabling it to influence a wide range of conformations in a pairwise non-additive manner. We will show that this modification produces intriguing effects on folding cooperativity and the rate-topology dependence of the protein model.

II. MODEL AND METHODS

We model proteins as self-avoiding chains on a three-dimensional cubic lattice with Gō potentials⁵¹ for contacts between the residues and an implicit solvent. The proteins are of the same length of 27 residues and have the native states being $3 \times 3 \times 3$ compact conformations (see an example of a native conformation in Fig. 1(a)). The energy of a protein in a given conformation is given by

$$E = -n_c \varepsilon + n_0 \varepsilon_s, \quad (1)$$

where n_c is the number of native contacts, $\varepsilon > 0$ is an energy unit in the system with $-\varepsilon$ being the energy of a native contact; n_0 is the number of residues that make no contacts with other residues, considered as the number of fully solvent-exposed residues (see example in Fig. 1 (b));

and ε_s is the solvation energy per fully solvent-exposed residue. In a given protein conformation n_c is given by

$$n_c = \sum_{i < j-1} \Delta_{ij} \Delta_{ij}^{\text{NAT}}, \quad (2)$$

where Δ is a protein contact map in the given conformation with Δ_{ij} equal to 1 if two residues i and j are nearest neighbors on the lattice but not consecutive along the chain, and 0 otherwise; Δ^{NAT} is the contact map of the native conformation. We generally consider $\varepsilon_s \leq 0$, but also some positive values of ε_s for comparison. For $\varepsilon_s = 0$, the model becomes identical to the Gō model⁵⁷.

The relative contact order parameter (RCO)²⁷ of a native state is defined as

$$RCO = \frac{\sum_{i < j-1} \Delta_{ij}^{\text{NAT}} |i - j|}{N \sum_{i < j-1} \Delta_{ij}^{\text{NAT}}}. \quad (3)$$

There are 97 distinct values of RCO ranging from about 0.28 to about 0.53 for $3 \times 3 \times 3$ compact conformations⁴¹. Our set of proteins corresponds to 97 different native states, such that for each RCO value there is only one native state picked up randomly from the compact conformations. The number of native contacts is $n_c = 28$ for all maximally compact lattice proteins.

Our Monte Carlo (MC) simulations follow the Metropolis algorithm⁵⁸ and the standard polymer move set, which contains single monomer moves (corner flip and end move) and double monomer moves (crankshaft)⁵⁹. The single and double monomer moves were attempted with probabilities of 0.2 and 0.8, respectively. For calculating thermodynamic properties, we employed the replica-exchange technique⁶⁰ in parallel tempering simulations and the weighted histogram method⁶¹ in the data analyses. The specific heat of a protein is given by

$$C(T) = \frac{\langle E^2 \rangle - \langle E \rangle^2}{k_B T^2}, \quad (4)$$

where $\langle \cdot \rangle$ denotes a thermodynamic average, k_B is the Boltzmann constant, and T is an absolute temperature. In our consideration, T is given in units of ε/k_B .

Kinetic properties were obtained from independent folding and unfolding trajectories in multiple simulations. The folding trajectories start from random conformations sampled at infinite temperatures and proceed until the native state is reached. The unfolding trajectories start from the native state and proceed until the number of native contacts is less than 20% of that of the native state. The folding and unfolding rates (k_f and k_u) are determined as the inverse of the median folding and unfolding times, respectively. Time is measured in MC steps.

III. RESULTS

We began by studying the effects of solvation on the folding properties of proteins. For a detailed analysis,

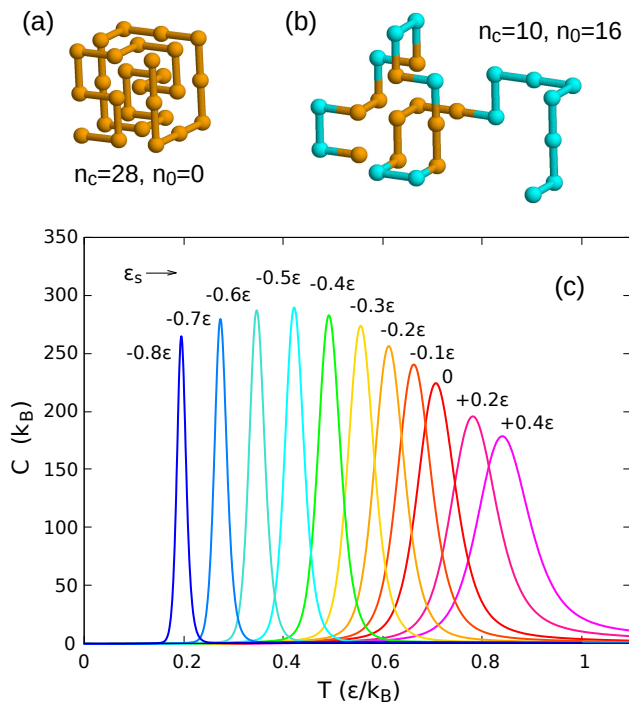


FIG. 1. Examples of lattice protein conformations of 27 residues: (a) a compact native state and (b) a partially unfolded conformation. In these visualizations, residues in contact with other residues are shown in orange, while residues fully exposed to the solvent are shown in cyan. The number of native contacts (n_c) and the number of fully exposed residues (n_0) for each conformation are indicated. (c) Temperature dependence of the specific heat for the model protein with the native state shown in (a), for various values of the solvation energy parameter ϵ_s ranging between -0.8ϵ and $+0.4\epsilon$, as indicated.

we selected a representative protein with an intermediate RCO value. The native state of this protein is illustrated in Fig. 1(a), and its corresponding RCO value is 0.4048. We calculated the temperature dependence of the specific heat for this protein at various values of ϵ_s , between -0.8ϵ and $+0.4\epsilon$. Fig. 1(c) shows that as ϵ_s decreases, the peak of the specific heat shifts to lower temperatures and becomes sharper. The increased sharpness of the peak with decreasing ϵ_s is accompanied by a reduced width and an increased height of the peak; however, the height reaches its maximum at $\epsilon_s \approx -0.5\epsilon$ and then decreases. These remarkable changes in the specific heat peak indicate that solvation significantly influences the folding transition.

The cooperativity of the folding transition can be assessed from the specific heat data. We followed Privalov and Potekhin⁶², and Kaya and Chan^{24,25}, to calculate the ratio $\kappa = \Delta H_{\text{vh}}/\Delta H_{\text{cal}}$ between the van't Hoff enthalpy (ΔH_{vh}) and the calorimetric enthalpy (ΔH_{cal}) from the specific heat. The experimental calorimetric criterion requires $\kappa = 1$ for a two-state process⁶². Two-state proteins have κ within the range of 1 ± 0.05 ^{21,62}.

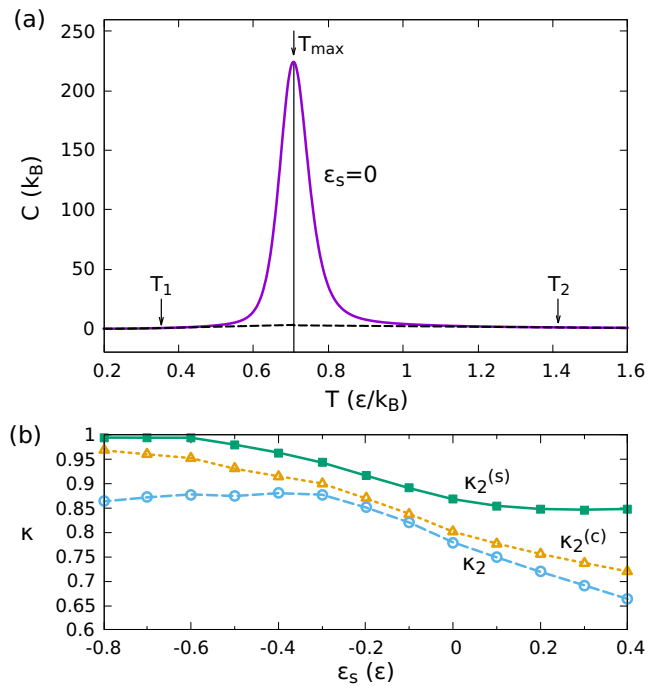


FIG. 2. (a) The specific heat as a function of temperature, $C(T)$, for the model protein in Fig. 1 with $\epsilon_s = 0$, is shown with baselines (dashed) for the folded and unfolded states. The latter are defined as straight lines tangent to the curve $C(T)$ at a low temperature T_1 and a high temperature T_2 , respectively, and extending between these temperatures and the temperature of the specific heat maximum, T_{max} . For $T < T_1$ and $T > T_2$, the baseline is the same as $C(T)$. For convenience, we have chosen $T_1 = 0.5 T_{\text{max}}$ and $T_2 = 2 T_{\text{max}}$. (b) Dependence of the cooperativity index κ , calculated with a baseline subtraction ($\kappa_2^{(s)}$ (squares)) and without baseline subtraction (κ_2 (circles) and $\kappa_2^{(c)}$ (triangles)) from the specific heat, on the solvation energy parameter ϵ_s , for the same protein as in (a).

Though the calorimetric criterion itself is not sufficient for determining a two-state process⁶³, κ may be considered as a measure of thermodynamic cooperativity^{24,25}. Without a baseline subtraction from the specific heat, κ can be given by^{25,62} $\kappa_2 = 2T_{\text{max}}\sqrt{k_B C_{\text{max}}}/\Delta H_{\text{cal}}$ with $\Delta H_{\text{cal}} = \int_0^\infty C(T)dT$, where C_{max} and T_{max} are the specific heat maximum and its temperature. In our numerical calculation of ΔH_{cal} , the integration of $C(T)$ is taken with T running from 0 to $5T_{\text{max}}$. When a baseline subtraction is applied, κ is equal to $\kappa_2^{(s)}$, as given in Ref.²⁵ under the same notation. Our construction of the baselines (see Fig. 2(a) and its caption) is similar to that described in Ref.²⁵, with an addition that we specified the two temperatures, where the baselines for the folded and unfolded states are tangent to the specific heat curve, to be given by $T_1 = 0.5T_{\text{max}}$ and $T_2 = 2T_{\text{max}}$, respectively. We defined also another cooperativity index, denoted as $\kappa_2^{(c)}$, which is without baseline subtraction but with $\Delta H_{\text{cal}} = \int_{T_1}^{T_2} C(T)dT$. By comparing $\kappa_2^{(c)}$ to κ_2 and

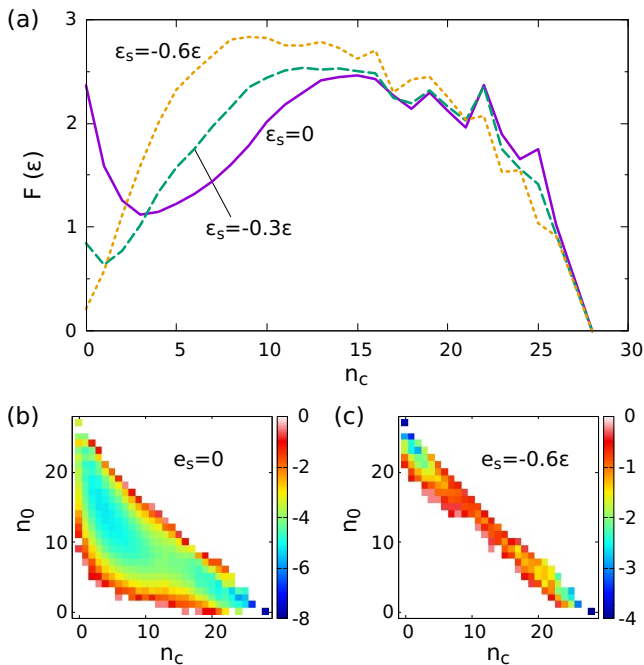


FIG. 3. (a) The free energy F as a function of the number of native contacts n_c at the temperature $T = T_{\max}$ for the protein with the native state shown in Fig. 1(a), with the solvation energy parameter $\epsilon_s = 0$ (solid), $\epsilon_s = -0.3\epsilon$ (dashed) and $\epsilon_s = -0.6\epsilon$ (dotted). F is calculated as $F(n_c) = -k_B T_{\max} \log P(n_c)$, where $P(n_c)$ is the probability of finding a conformation with n_c native contacts, obtained from a long MC simulation at $T = T_{\max}$. (b and c) The free energy as a function of n_c and the number of fully solvent-exposed residues n_0 , shown as color maps for the two cases: $\epsilon_s = 0$ (b) and $\epsilon_s = -0.6\epsilon$ (c). The maps were calculated using the same simulation data as in (a). The native state corresponds to the state with $n_c = 28$ and $n_0 = 0$.

$\kappa_2^{(s)}$, one can see separately the effects of the temperature range and of the baselines, respectively, on their values. The numerical values of $\kappa_2^{(c)}$ and $\kappa_2^{(s)}$ depend on the choice of T_1 and T_2 , and it is not clear how to determine the correct values. Our aim here is to show how they qualitatively depend on ϵ_s .

Figure 2(b) shows that as ϵ_s decreases from 0.4ϵ to -0.8ϵ , $\kappa_2^{(s)}$ monotonically increases from approximately 0.85 to more than 0.99. $\kappa_2^{(c)}$ also monotonically increases to a value larger than 0.96, while κ_2 only increases from 0.66 to a maximum of about 0.88 at $\epsilon_s = -0.4\epsilon$ and then slightly decreases. The main reason why κ_2 decreases is that at low ϵ_s , the specific heat develops a long tail at high temperatures, leading to an increase in the calculated calorimetric enthalpy. Therefore, $\kappa_2^{(s)}$ and $\kappa_2^{(c)}$ may be more meaningful than κ_2 in underscoring the folding transition for low values of ϵ_s . Both the behaviors of $\kappa_2^{(s)}$ and $\kappa_2^{(c)}$ indicate a significant increase of folding cooperativity upon decreasing the solvation energy parameter.

The effect of solvation on folding cooperativity can be

understood by examining the free energy profiles of the protein (Fig. 3). These profiles show that a negative solvation energy shifts the unfolded state and the transition state further away from the native state along the folding coordinate, increases the folding free energy barrier, and narrows the folding pathways. Specifically, Fig. 3(a) shows that while the native state remains unchanged, the unfolded state, corresponding to the free energy minimum at a small number of native contacts n_c , is shifted toward lower values of n_c and also lower values of the free energy F as ϵ_s decreases from zero to -0.6ϵ . At the same time, the transition state, which presumably corresponds to the maximum of the largest free energy barrier, is shifted toward lower values of n_c and higher values of F . Due to these shiftings, the folding free energy barrier, ΔF_U^\ddagger , given by the free energy difference between the transition state (\ddagger) and the unfolded state (U), obtained at $T = T_{\max}$, is increased almost twice (from $\sim 1.34\epsilon$ to $\sim 2.62\epsilon$) as ϵ_s decreases from zero to -0.6ϵ . Since T_{\max} also decreases with ϵ_s (see Fig. 1), the increase of ΔF_U^\ddagger in units of $k_B T$ is about 4 times as ϵ_s decreases from zero to -0.6ϵ . Figures 3 (b and c) show that the pathway between the native state and the unfolded state is narrowed due to the effect of a negative solvation energy, as the latter energetically disfavors conformations with low values of n_0 , the number of fully solvent-exposed residues. Because non-native contacts have zero energy, they are strongly disfavored by the negative solvation energy if their formation decreases n_0 . Both the increased free energy barrier and the narrowed folding pathway promote folding cooperativity, as they make the accessible states on the pathway connecting the unfolded and native states less probable, making the system more two-state-like. We have checked that the linear shape of folding pathway in the n_0 - n_c plan shown in Fig. 3c is also found in other lattice proteins for the same value of ϵ_s .

One can think of varying the solvation energy parameter as a way to mimic the effect of denaturants. We determined the folding and unfolding rates, k_f and k_u , at two different temperatures, $T = 0.5 \epsilon/k_B$ and $T = 0.3 \epsilon/k_B$, from the simulations of the selected protein for various values of ϵ_s . Using these data, we constructed chevron plots of $\log k_f$ and $\log k_u$ vs. $-\epsilon_s$, where $-\epsilon_s$ represents the effect of increasing denaturant concentration (Fig. 4). Note that the pure solvent may correspond to a specific value of ϵ_s , and the presence of a denaturant adds to that value. Figure 4 shows that as the temperature decreases, the V-shaped region around the denaturation midpoint shifts toward higher values of $-\epsilon_s$ and lower values of k_f and k_u . The linear fits of $\log k_f$ and $\log k_u$ vs. $-\epsilon_s$ near the denaturation midpoint are indications of two-state folding kinetics. Note that these linear fits are better defined, spanning a wider range of $-\epsilon_s$, at $T = 0.3 \epsilon/k_B$ than at $T = 0.5 \epsilon/k_B$. This indicates that the kinetic data align more closely with the two-state model in the lower range of ϵ_s . Experimentally, the movements of the denaturation midpoint towards higher denaturant concentration and lower values of transition rates on de-

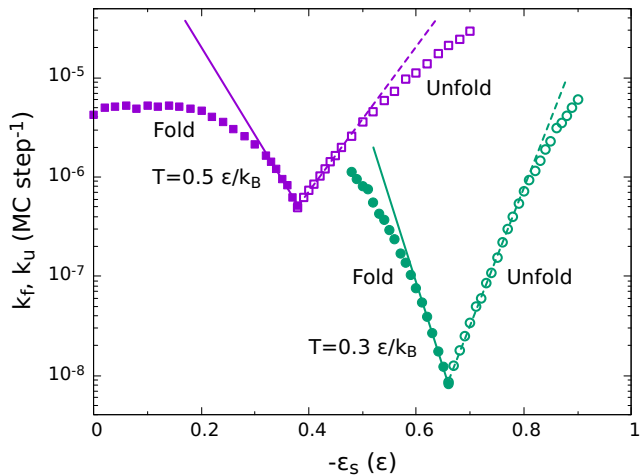


FIG. 4. Chevron plots of the folding (filled symbols) and unfolding (open symbols) rates as functions of the solvation energy parameter ε_s for the protein with the native state shown in Fig. 1(a) at two different temperatures, $T = 0.5 \varepsilon/k_B$ (squares) and $T = 0.3 \varepsilon/k_B$ (circles). The folding (k_f) and unfolding (k_u) rates, shown on a logarithmic scale, are defined as the inverse of the median folding (unfolding) time obtained from the simulations. For each temperature and each value of ε_s , k_f and k_u are determined from 1001 independent trajectories. Data points near the chevron turnover are fitted by linear functions for the folding (solid line) and unfolding (dashed line) rates separately.

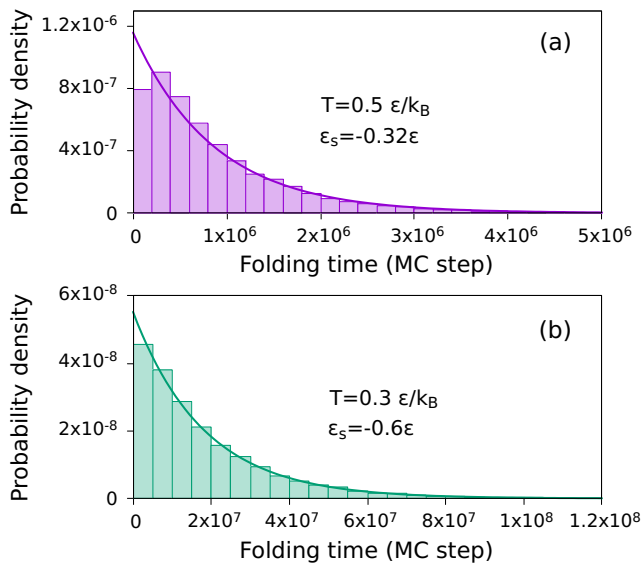


FIG. 5. Normalized histograms of the folding times (boxes) for the protein considered in Fig. 4 at two different conditions of temperature and solvation energy: (a) $T = 0.5 \varepsilon/k_B$, $\varepsilon_s = -0.32\varepsilon$; and (b) $T = 0.3 \varepsilon/k_B$, $\varepsilon_s = -0.6\varepsilon$. The folding times in each plot are obtained from simulations of 10,000 independent folding trajectories. The histograms are plotted against the exponential distribution $g(t) = t_a^{-1} \exp(-t/t_a)$ (solid line) of the folding time t , where t_a is the average folding time calculated from the simulation data.

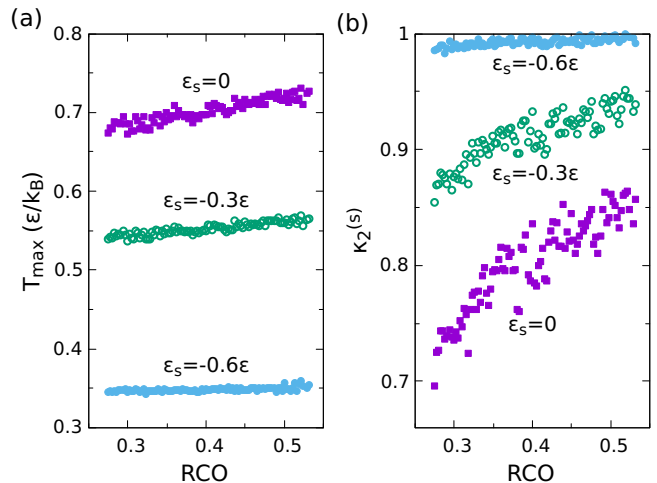


FIG. 6. Temperature of the maximum of the specific heat, T_{\max} , (a) and the cooperativity index $\kappa_2^{(s)}$ (b) of 97 lattice proteins considered are plotted against their relative contact order (RCO) for three values of the solvation energy parameter: $\varepsilon_s = 0$ (filled squares), -0.3ε (open circles) and -0.6ε (filled circles), as indicated.

creasing temperature have been observed, e.g. for the N-terminal domain of L9 protein^{64,65}. For this protein, no rollover of the chevron plots was observed, even at low concentrations of denaturant, for temperatures between 9°C and 40°C^{64,65}, indicating a very high two-state kinetic cooperativity that remains unchanged within this range of temperature. For temperatures above 55°C, the range of denaturant concentration at which the rates can be measured is significantly reduced⁶⁴, which somewhat aligns with our simulation results.

Figure 5 shows that the histograms of the folding times obtained from simulations for the temperature and solvation energy parameters, T and ε_s , within the linear regions of the corresponding chevron plots in Fig. 4, align well with an exponential distribution of folding time, which is characteristic of the kinetics of a two-state system²². Notably, the histogram at $T = 0.3 \varepsilon/k_B$ and $\varepsilon_s = -0.6\varepsilon$ (Fig. 5b) fits the exponential function slightly better at low time values than the one at $T = 0.5 \varepsilon/k_B$ and $\varepsilon_s = -0.32\varepsilon$ (Fig. 5a), indicating an increased two-state cooperativity at the lower ε_s value.

We now turn to examining the effect of solvation on the correlations between folding properties and the relative contact order. To this end, we considered 97 model proteins with distinct RCO values and determined their specific heats and folding rates through simulations. Figure 6a shows that the temperature T_{\max} , corresponding to the maximum of the specific heat of the proteins, increases weakly with RCO, albeit with some small variations. Without solvation, T_{\max} rises by approximately 8% as RCO increases from 0.28 to 0.53. With solvation, the rise decreases to about 6% for $\varepsilon_s = -0.3\varepsilon$ and about 4% for $\varepsilon_s = -0.6\varepsilon$. Fig. 6b shows that the co-

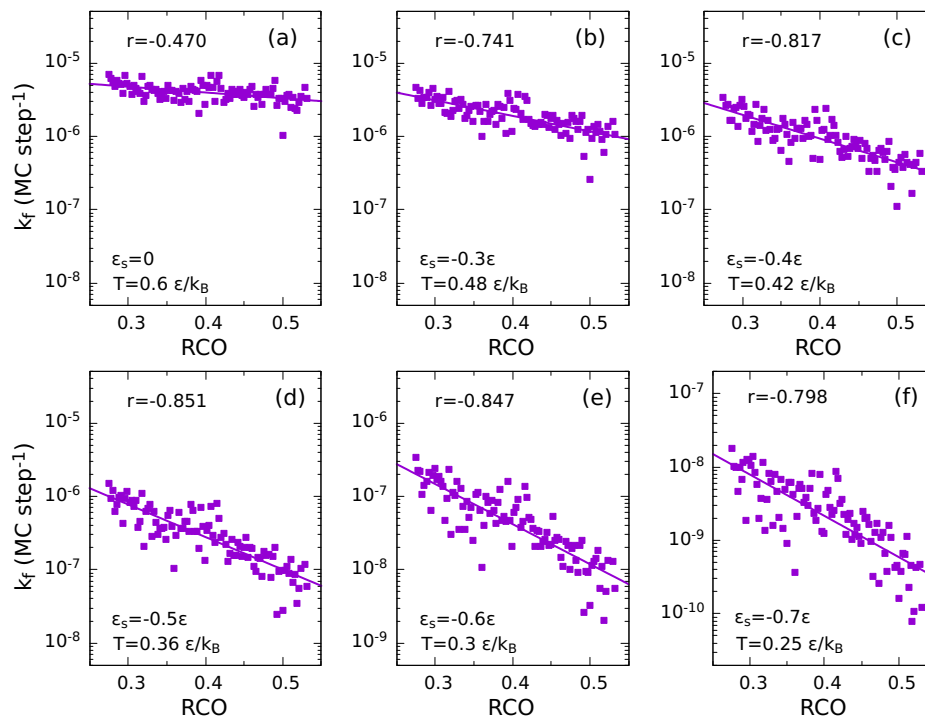


FIG. 7. Folding rate (k_f), on a logarithmic scale, vs. the relative contact order (RCO) of 97 lattice proteins, as considered in Fig. 6, is shown for 6 cases (a–f) with different values of ε_s and T , as indicated. A linear fit to the data points (solid line) and the correlation coefficient r are provided in each plot. The corresponding p -value is smaller than 10^{-5} in all cases. Each data point was obtained from 201 independent folding trajectories.

operativity index with a baseline subtraction, $\kappa_2^{(s)}$, on average, increases with RCO. Interestingly, the RCO dependence of this cooperativity index is strongest for the case without solvation, $\varepsilon_s = 0$, and weakens as ε_s decreases below zero. Similar trends are also found for κ_2 and $\kappa_2^{(c)}$ (data not shown). These results indicate that proteins with higher RCO in general are thermally more stable and have higher folding cooperativity than those with lower RCO. It is also shown that solvation weakens the RCO dependence of both thermal stability and folding cooperativity, even though it enhances folding cooperativity. These behaviors can be rationalized as being due to the stabilizing effect of short-range native contacts (along the sequence). In the absence of the solvation term, a larger number of such contacts are expected to be present in conformations of the unfolded state for proteins with lower RCO, leading to an increased stability of the unfolded state and consequently a lower folding temperature. More of these contacts also contribute to the stability of partially folded conformations, leading to a decreased folding cooperativity for proteins with lower RCO. In the presence of the solvation energy term, the effect of short-range native contacts is diminished by competing solvent interactions.

To examine the effect of solvation on the rate-topology dependence, we determined the folding rates, k_f , at constant temperatures T 's below T_{\max} for all 97 proteins. We found that the best correlation between $\log k_f$ and RCO

occurs when T is in the range from $0.85\bar{T}_{\max}$ to $0.9\bar{T}_{\max}$, where \bar{T}_{\max} is the mean value of T_{\max} of all the proteins at a given ε_s . Figure 7 shows the dependence of $\log k_f$ on RCO at temperatures within this ‘optimal’ range for various values of ε_s . For each value of ε_s , this rate-topology dependence is shown for a fixed temperature T for all proteins to mimic a real situation, as if the folding rates of all proteins were measured under the same solvent conditions. In this figure, one observes not only the tendency of $\log k_f$ to decrease with RCO in all the cases, but also the increase the slope of the linear regression between $\log k_f$ and RCO as ε_s decreases. The diversity of the folding rates increases from less than one order of magnitude for $\varepsilon_s = 0$ to more than two orders of magnitude for $\varepsilon_s = -0.7\varepsilon$. The correlation between $\log k_f$ and RCO improves significantly as ε_s decreases, with the correlation coefficient r rising from -0.470 to -0.851 as ε_s decreases from 0 to -0.5ε (Figs. 7a to 7d). However, the correlation somewhat decreases when ε_s becomes smaller than -0.5ε , but remains high at $\varepsilon_s = -0.6\varepsilon$ and -0.7ε (Figs. 7e and 7f). The slope of the $\log k_f$ vs. RCO dependence, the correlation coefficient r and the p -value for all cases studied with different values of ε_s are listed in Table I.

The best correlation obtained in the present study ($r \approx -0.85$) is better than that in the study of Jewett et al.⁴¹ ($r \approx -0.75$), but somewhat lower than that in the work of Kaya and Chan⁴² ($r \approx -0.91$), for similar lattice systems but with different models. The increase in the diversity

TABLE I. Summary of the solvation dependence of folding cooperativity and the folding rate-topology correlation obtained from simulations for 97 lattice proteins. For each value of the solvation energy parameter ε_s , the data shown correspond to the mean values of the cooperativity indices κ_2 , $\kappa_2^{(c)}$, and $\kappa_2^{(s)}$, as well as the temperature of the specific heat maximum, T_{\max} , averaged over all 97 proteins (the average is denoted by a bar above each symbol). Additionally, the temperature T at which the folding rates k_f of the proteins were determined, the slope of the dependence of $\log k_f$ on RCO, the Pearson’s correlation coefficient r , and the corresponding p -value are provided.

$\varepsilon_s (\varepsilon)$	$\bar{\kappa}_2$	$\bar{\kappa}_2^{(c)}$	$\bar{\kappa}_2^{(s)}$	$\bar{T}_{\max} (\varepsilon/k_B)$	$T (\varepsilon/k_B)$	Slope of $\log k_f$ vs. RCO	r	p -value
0.0	0.802	0.826	0.890	0.702	0.60	-0.79 ± 0.15	-0.470	$< 10^{-5}$
-0.1	0.839	0.858	0.908	0.658	0.57	-0.98 ± 0.16	-0.521	$< 10^{-5}$
-0.2	0.866	0.886	0.929	0.609	0.53	-1.26 ± 0.18	-0.628	$< 10^{-5}$
-0.3	0.888	0.912	0.952	0.553	0.48	-2.11 ± 0.20	-0.741	$< 10^{-5}$
-0.4	0.887	0.923	0.969	0.490	0.42	-3.24 ± 0.23	-0.818	$< 10^{-5}$
-0.5	0.875	0.929	0.983	0.423	0.36	-4.44 ± 0.28	-0.851	$< 10^{-5}$
-0.6	0.868	0.949	0.993	0.355	0.30	-5.46 ± 0.35	-0.847	$< 10^{-5}$
-0.7	0.850	0.950	0.995	0.295	0.25	-5.62 ± 0.44	-0.798	$< 10^{-5}$

of the folding rates due to the effect of solvation in our study is not too impressive but comparable to those in the previous studies^{41,42}.

We have also calculated the average values of various cooperativity indices, $\bar{\kappa}_2$, $\bar{\kappa}_2^{(c)}$, and $\bar{\kappa}_2^{(s)}$, across all 97 proteins, for different values of ε_s (see Table I). The dependences of these average indices on ε_s are similar to that shown in Fig. 2(b). We found that the correlation coefficient r as well as the slope of the $\log k_f$ vs. RCO dependence strongly correlate with both $\bar{\kappa}_2^{(c)}$ and $\bar{\kappa}_2^{(s)}$, whereas it shows a medium correlation with $\bar{\kappa}_2$. In particular, the corresponding correlation coefficient exceeds 0.96 for r vs. $\bar{\kappa}_2^{(c)}$ and r vs. $\bar{\kappa}_2^{(s)}$, and is about 0.78 for r vs. $\bar{\kappa}_2$. Thus, the non-monotonic trends observed in the dependencies of $\bar{\kappa}_2$ and r on ε_s seem to be weakly related. The strong correlations of r with $\bar{\kappa}_2^{(c)}$ and $\bar{\kappa}_2^{(s)}$ support the idea that the folding rate-topology dependence is linked to folding cooperativity⁴¹.

IV. DISCUSSION

Although a more appropriate way to theoretically study protein folding would be to start with a sequence-based model and select foldable sequences through an evolutionary sequence design^{66,67}, in this work, we adhere to the Gō model due to the significant success of its structure-based approach in capturing protein folding mechanisms⁵⁵ and its relatively well-known folding properties³¹. Because Gō model is minimally frustrated⁶⁸, its energy landscape is smooth and funnel-like⁶⁹, facilitating rapid folding, as expected for globular proteins. The folding rate in the Gō model is close to that of the fastest-folding sequence in a comparable sequence-based model for a given native structure^{70,71}. Gō model is also often more cooperative than its sequence-based counterparts²⁵. Using the Gō model, the solvation effects on folding cooperativity and the rate-topology dependence can be studied without perturbations from the

sequence²⁸. For the type of solvation energy considered, the solvation effects can be expected to be independent of the sequence. Thus, for sequence-based models, the effects of solvation can be qualitatively similar to those obtained with the Gō model.

To some extent, the favorable solvation energy for fully exposed residues in our model may correspond to the solvation of peptide groups (-NHCO-) in the protein backbone. Experimental transfer data of amides indicate that the polar interaction between water and peptide CO and NH groups is entirely enthalpic with the hydration enthalpy as low as -11.6 kcal/mol for a free amide group⁴. Electrostatic solvation free energy (ESF) calculation based on numerically solving the Poisson-Boltzmann equation⁷² gives an ESF of -7.9 kcal/mol for an alanine peptide group in the solvent-exposed β -strand conformation, and -2.5 kcal/mol for a hydrogen-bonded (H-bonded) peptide group in a solvent-exposed alanine α -helix⁷³. A similar ESF of -2.5 kcal/mol was found also for an alanine H-bonded peptide group in an alanine β -hairpin^{74,75}. Other non-polar amino acids may have higher ESF values (negative but closer to zero) for their peptide groups in α - and β -structures than alanine due to more effective side-chain shielding of the peptide backbone⁴. These data indicate that the desolvation of a peptide group due to secondary structure formation increases the hydration enthalpy by at least 5.4 kcal/mol. This energy penalty is significantly large compared to an average contribution of hydrophobic interaction, which has been estimated to be about -1.25 kcal/mol per residue⁷⁵, based on the calculation of buried nonpolar surface areas. If the secondary structures form prior to the tertiary structure^{37,53,76}, then for most residues, the first contact with another residue would correspond to the formation of a peptide H-bond, which causes a substantial desolvation of the peptide group. In our model, a peptide H-bond is considered as a native interaction. A residue can undergo multiple stages of desolvation during the folding process. The above consideration suggests that the initial stage of desolvating the peptide group due

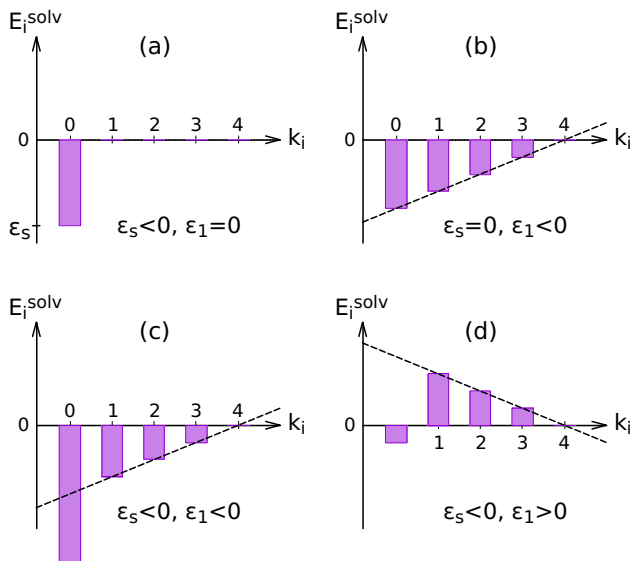


FIG. 8. Different shapes of the solvation potential, shown as dependence of the residual solvation energy (E_i^{solv}) on the number of residue-residue contacts (k_i) of a non-terminal residue. E_i^{solv} is obtained from Eq. (5) for different choices of parameters: (a) $\varepsilon_1 = 0$, $\varepsilon_s < 0$; (b) $\varepsilon_1 < 0$, $\varepsilon_s = 0$; (c) $\varepsilon_1 < 0$, $\varepsilon_s < 0$; and (d) $\varepsilon_1 > 0$, $\varepsilon_s < 0$; The energy unit is arbitrary. The linear part of the potential is indicated by a dashed line.

to peptide H-bond formation is associated with the most significant change in the hydration enthalpy. The singular term in our solvation potential is supported by this assessment.

One can think of a more general form of the considered solvation potential, which covers also partially exposed residues. Let k_i be the number of contacts made by residue i in a given conformation; k_i takes integer values from 0 to k_i^{max} , where k_i^{max} is equal to 4 and 5 for non-terminal and terminal residues, respectively, on the cubic lattice. It follows that $\sum_i k_i = 2(n_c + n_{nn})$ and $\sum_i \delta_{k_i,0} = n_0$, where n_{nn} is the number of non-native contacts, and $\delta_{k,l}$ is the Kronecker's delta function. Consider the residual solvation energy as a function of k_i in the form:

$$E_i^{\text{solv}} = (k_i^{\text{max}} - k_i)\varepsilon_1 + \delta_{k_i,0}\varepsilon_s, \quad (5)$$

where $(k_i^{\text{max}} - k_i)$ represents the exposure degree of the residue i , and ε_1 is an energy parameter. Incorporating the solvation potential in Eq. (5) into the G \bar{o} model gives the total energy

$$E = -n_c(\varepsilon + 2\varepsilon_1) - 2n_{nn}\varepsilon_1 + n_0\varepsilon_s + \text{const.}, \quad (6)$$

where the additive constant does not depend on the chain conformation. Thus, the linear term in Eq. (5) is interchangeable with the energies of native and non-native contacts, and therefore can be absorbed into the G \bar{o} model with energy contributions from non-native contacts.

Figure 8 shows various shapes of the solvation potential in Eq. (5) for several choices of the parameters ε_s and ε_1 . We have checked that the solvation potential in Fig. 8b ($\varepsilon_s = 0$, $\varepsilon_1 < 0$) enhances the folding cooperativity of the G \bar{o} model in a similar manner to what obtained by the potential in Fig. 8a ($\varepsilon_s < 0$, $\varepsilon_1 = 0$), but to a significantly lower degree. In particular, by using the same analysis of the specific heats as shown in Fig. 2, as ε_1 decreases towards more negative values, the cooperativity index $\kappa_2^{(s)}$ increases only up to a maximum of 0.91, while κ_2 reaches a maximum of 0.81. It is expected that the potential in Fig. 8c ($\varepsilon_s < 0$, $\varepsilon_1 < 0$) can improve the folding cooperativity as effectively as the potential in Fig. 8a, while the potential in Fig. 8d ($\varepsilon_s < 0$, $\varepsilon_1 > 0$) may be less effective than the latter. This expectation is based on the observation that the competition between solvation and native interactions promotes cooperativity.

The derivation of Eq. (6) is similar to the treatment of polymer-solvent interactions in the Flory-Huggins theory⁷⁷. It indicates that if the solvation potential is a linear function of the number of residue-residue contacts then the solvation energy remains pairwise additive. In our model, pairwise non-additivity⁶ comes from a singular term for the solvation of fully exposed residues, which makes the solvation potential nonlinear. In traditional implicit solvent models⁷⁸, the solvation free energy of a solute is often assumed to be proportional to the solvent accessible surface area (SASA)⁷⁹ of its molecular surface. Depending on the solvent molecule radius, SASA can be a nonlinear function of the number of residue-residue contacts due to the overlaps of buried areas arising from different contacts⁸⁰. The nonlinearity of a solvation potential for a residue may also arise from the irregular shape of the residue and the anisotropy of its surface¹⁷. For example, the surface of an amino acid residue can have both polar and nonpolar regions, which contribute differently to the solvation energy.

Several solvation models have been proposed in the past to capture the effects of water on protein folding. Early simulations of lattice protein models by Hao and Scheraga¹⁷ have shown that adding a solvation term to pairwise contact potentials improves the foldability of sequences and makes the folding transition first-order like. Their solvation model specifies a preferred solvation state for each residue and applies an increasing energy penalty for solvation states that deviate from the preferred state. Using the Hao and Scheraga's model and a two-letter sequence design, Sorenson and Head-Gordon found that sequences in the solvation model fold faster and more cooperative than sequences in the nonsolvation model¹⁸. Note that Hao and Scheraga's solvation potential is also nonlinear, depending on the type of amino acid, but it has no singular term as in our potential. Using a coarse-grained model for protein structure prediction, Wolynes and coworkers⁷ demonstrated that adding nonpairwise-additive water-mediated knowledge-based interactions to the Hamiltonian markedly improves the quality of structure prediction. Their solvation model includes a water-

mediated second-well potential that depends on the local density environment of residues and facilitates residue-residue indirect contact at an intermediate C_{β} - C_{β} distance (6.5–9.5 Å), mimicking the effect of one or two water layers between the residues. This potential provides a ‘wetting’ of non-buried residues, but unlike our solvation potential, it has a distance constraint on the interacting residues, therefore promoting intermediate chain compaction. The studies of Chan and coworkers^{12,13,44–47} showed that Gō-like models with desolvation barriers embedded in the native contact potentials^{11,13} possess higher degrees of folding cooperativity than models without the desolvation barriers. These barriers account for the process of the hydration water expulsion when residues come into a direct contact¹⁰. It was shown that their effects on folding cooperativity can be very strong and may be intimately linked to the shortening of the effective attractive range of residue-residue interactions⁴⁷. Note that both the second-well potential and the desolvation barrier potential in these previous works promote solvent-induced interactions at an intermediate to short range of distance between the residues, while our solvation energy applies to fully exposed residues regardless of their distance from each other. However, a favorable interaction with the solvent is implied in both our and their models. The successes of all these previous approaches demonstrate the significant role of water in various details of the folding process^{10,81}. Our study further supports this perspective.

Our study aligns with previous studies of lattice models, which showed that higher folding cooperativity is associated with a stronger topology dependence of the folding rates^{41,42}. However, other studies of off-lattice models indicated that while cooperativity increases folding rate diversity, it does not necessarily enhance the rate-topology dependence^{44–47}. The mechanism behind the folding rate-topology dependence may lie beyond the energetics^{35–38,43}. Notably, a model based on the “zip-ping up” mechanism, using a few physical rate parameters, can predict the folding rates of two-state proteins from their native contact maps with good correlation to experimental data³⁷. This mechanism is defined by a time sequence of folding events supported by molecular dynamics simulations of a Gō-like model^{52,53}. A number of studies have been focused on the topological aspect of the rate-topology relation. In addition to RCO, several descriptors have been proposed to predict folding rates from the native state structures, including long-range order⁸², the number of native contacts⁸³, total contact distance⁸⁴, absolute contact order⁸⁵, cliquishness⁸⁶, local secondary structure content⁸⁷, and relative logarithmic effective contact order⁸⁸. Although their performance typically does not surpass that of RCO for two-state proteins, some are effective for both two- and three-state proteins^{84–86}. Recently, it was shown that maximum intrachain contact entanglement⁸⁹, a new descriptor of protein native state entanglement, can improve the folding rate predictions when combined with other descriptors,

underscoring the importance of topological complexity beyond contact order.

V. CONCLUSION

We have introduced a solvation energy into the lattice Gō model, which favors residues that are fully exposed to the solvent. This solvation energy promotes unfolding of proteins and is meant to compensate for the overwhelming native bias in the Gō model which considers only native interactions. Our results show that it significantly enhances both the folding cooperativity and the folding rate-topology dependence of the lattice proteins considered, thereby suggesting that this type of solvent interactions may play a key role in determining these properties in two-state proteins.

The mechanism by which the competition between the solvation and native interactions enhances folding cooperativity has been elucidated. We have demonstrated that as the solvation energy parameter decreases, the folding free energy barrier increases. This occurs due to a decrease in the free energy of the unfolded state together with an increase in the free energy of the transition state. In addition, the folding pathways become narrower because the solvation potential energetically disfavors the formation of non-native contacts. The heightened folding free energy barrier and the narrowed folding routes strengthens folding cooperativity by making the system more two-state-like.

We have also suggested that the solvation energy in our model corresponds to the solvation of peptide groups in the protein backbone. The polar interaction between water and exposed peptide groups is highly favorable. Peptide groups become substantially desolvated due to peptide hydrogen bonding during secondary structure formation, resulting in a substantial deficit in hydration enthalpy. Our study indicates that the effects of peptide group solvation can be significant for the protein folding cooperativity and for the folding rate-topology dependence. It is expected that these effects can be studied in more realistic models.

ACKNOWLEDGEMENTS

This work is dedicated to Marek Cieplak and is supported by Vietnam Academy of Science and Technology under Grant No. NCXS02.05/22-23. The simulations were conducted using the HPC cluster at IOP-VAST.

AUTHOR DECLARATIONS

Conflict of interest

The authors have no conflicts to disclose.

DATA AVAILABILITY STATEMENT

The data that support the findings of this study are available from the corresponding author upon reasonable request.

- ¹W. Kauzmann, in *Advances in Protein Chemistry*, Vol. 14 (Elsevier, 1959) pp. 1–63.
- ²K. A. Dill, *Biochem.* **29**, 7133 (1990).
- ³R. L. Baldwin and G. D. Rose, *Proc. Natl. Acad. Sci. USA* **113**, 12462 (2016).
- ⁴P. Luo and R. L. Baldwin, *Proc. Natl. Acad. Sci. USA* **96**, 4930 (1999).
- ⁵D. Thirumalai, G. Reddy, and J. E. Straub, *Acc. Chem. Res.* **45**, 83 (2012).
- ⁶P.-Y. Morgantini and P. A. Kollman, *J. Am. Chem. Soc.* **117**, 6057 (1995).
- ⁷G. A. Papoian, J. Ulander, M. P. Eastwood, Z. Luthey-Schulten, and P. G. Wolynes, *Proc. Natl. Acad. Sci. USA* **101**, 3352 (2004).
- ⁸L. R. Pratt and D. Chandler, *J. Chem. Phys.* **67**, 3683 (1977).
- ⁹J. A. Rank and D. Baker, *Prot. Sci.* **6**, 347 (1997).
- ¹⁰Y. Levy and J. N. Onuchic, *Annu. Rev. Biophys. Biomol. Struct.* **35**, 389 (2006).
- ¹¹M. S. Cheung, A. E. García, and J. N. Onuchic, *Proc. Natl. Acad. Sci. USA* **99**, 685 (2002).
- ¹²H. Kaya and H. S. Chan, *J. Mol. Biol.* **326**, 911 (2003).
- ¹³Z. Liu and H. S. Chan, *J. Mol. Biol.* **349**, 872 (2005).
- ¹⁴S. E. Jackson and A. R. Fersht, *Biochem.* **30**, 10428 (1991).
- ¹⁵Y. M. Rhee, E. J. Sorin, G. Jayachandran, E. Lindahl, and V. S. Pande, *Proc. Natl. Acad. Sci. USA* **101**, 6456 (2004).
- ¹⁶K. Lindorff-Larsen, S. Piana, R. O. Dror, and D. E. Shaw, *Science* **334**, 517 (2011).
- ¹⁷M.-H. Hao and H. A. Scheraga, *Phys. A: Stat. Mech. Appl.* **244**, 124 (1997).
- ¹⁸J. M. Sorenson and T. Head-Gordon, *Fold. Des.* **3**, 523 (1998).
- ¹⁹Y. Snir and R. D. Kamien, *Science* **307**, 1067 (2005).
- ²⁰J. R. Banavar, T. X. Hoang, J. H. Maddocks, A. Maritan, C. Poletto, A. Stasiak, and A. Trovato, *Proc. Natl. Acad. Sci. USA* **104**, 17283 (2007).
- ²¹A. Viguera, J. Martinez, V. Filimonov, P. Mateo, and L. Serrano, *Biochem.* **33**, 2142 (1994).
- ²²K. W. Plaxco, J. I. Guijarro, C. J. Morton, M. Pitkeathly, I. D. Campbell, and C. M. Dobson, *Biochem.* **37**, 2529 (1998).
- ²³H. S. Chan, S. Shimizu, and H. Kaya, in *Methods in Enzymology*, Vol. 380 (Elsevier, 2004) pp. 350–379.
- ²⁴H. Kaya and H. S. Chan, *Phys. Rev. Lett.* **85**, 4823 (2000).
- ²⁵H. Kaya and H. S. Chan, *Prot. Struct. Func. Bio.* **40**, 637 (2000).
- ²⁶H. Kaya and H. S. Chan, *Phys. Rev. Lett.* **90**, 258104 (2003).
- ²⁷K. W. Plaxco, K. T. Simons, and D. Baker, *J. Mol. Biol.* **277**, 985 (1998).
- ²⁸K. W. Plaxco, K. T. Simons, I. Ruczinski, and D. Baker, *Biochem.* **39**, 11177 (2000).
- ²⁹D. Thirumalai, *J. Phys. I.* **5**, 1457 (1995).
- ³⁰A. M. Gutin, V. I. Abkevich, and E. I. Shakhnovich, *Phys. Rev. Lett.* **77**, 5433 (1996).
- ³¹M. Cieplak, T. X. Hoang, and M. S. Li, *Phys. Rev. Lett.* **83**, 1684 (1999).
- ³²M. Cieplak and T. X. Hoang, *J. Bio. Phys.* **26**, 273 (2000).
- ³³M. Cieplak and T. X. Hoang, *Prot. Struct. Func. Bio.* **44**, 20 (2001).
- ³⁴A. V. Finkelstein and A. Y. Badredtinov, *Fold. Des.* **2**, 115 (1997).
- ³⁵D. A. Debe and W. A. Goddard III, *J. Mol. Biol.* **294**, 619 (1999).
- ³⁶V. Muñoz and W. A. Eaton, *Proc. Natl. Acad. Sci. USA* **96**, 11311 (1999).
- ³⁷T. R. Weikl and K. A. Dill, *J. Mol. Biol.* **329**, 585 (2003).
- ³⁸D. E. Makarov and K. W. Plaxco, *Prot. Sci.* **12**, 17 (2003).
- ³⁹A. R. Fersht, *Proc. Natl. Acad. Sci. USA* **97**, 1525 (2000).
- ⁴⁰E. Paci, K. Lindorff-Larsen, C. M. Dobson, M. Karplus, and M. Vendruscolo, *J. Mol. Biol.* **352**, 495 (2005).
- ⁴¹A. I. Jewett, V. S. Pande, and K. W. Plaxco, *J. Biol. Mol.* **326**, 247 (2003).
- ⁴²H. Kaya and H. S. Chan, *Prot. Struct. Func. Gen.* **52**, 524 (2003).
- ⁴³S. Wallin and H. S. Chan, *Prot. Sci.* **14**, 1643 (2005).
- ⁴⁴A. Badasyan, Z. Liu, and H. S. Chan, *J. Mol. Biol.* **384**, 512 (2008).
- ⁴⁵A. Ferguson, Z. Liu, and H. S. Chan, *J. Mol. Biol.* **389**, 619 (2009).
- ⁴⁶H. S. Chan, Z. Zhang, S. Wallin, and Z. Liu, *Ann. Rev. Phys. Chem.* **62**, 301 (2011).
- ⁴⁷H. Kaya, Z. Uzunoglu, and H. S. Chan, *Phys. Rev. E* **88**, 044701 (2013).
- ⁴⁸N. Koga and S. Takada, *J. Mol. Biol.* **313**, 171 (2001).
- ⁴⁹M. Cieplak and T. X. Hoang, *Biophys. J.* **84**, 475 (2003).
- ⁵⁰M. Cieplak, *Phys. Rev. E* **69**, 031907 (2004).
- ⁵¹H. Taketomi, Y. Ueda, and N. Gō, *Int. J. Pep. Protein Res.* **7**, 445 (1975).
- ⁵²T. X. Hoang and M. Cieplak, *J. Chem. Phys.* **112**, 6851 (2000).
- ⁵³T. X. Hoang and M. Cieplak, *J. Chem. Phys.* **113**, 8319 (2000).
- ⁵⁴C. Clementi, H. Nymeyer, and J. N. Onuchic, *J. Mol. Biol.* **298**, 937 (2000).
- ⁵⁵D. Baker, *Nature* **405**, 39 (2000).
- ⁵⁶S. Takada, *Biophys. Physicobiology* **16**, 248 (2019).
- ⁵⁷H. Abe and N. Go, *Biopolymers* **20**, 1013 (1981).
- ⁵⁸N. Metropolis, A. W. Rosenbluth, M. N. Rosenbluth, A. H. Teller, and E. Teller, *J. Chem. Phys.* **21**, 1087 (1953).
- ⁵⁹M. Cieplak, M. Henkel, J. Karbowski, and J. R. Banavar, *Phys. Rev. Lett.* **80**, 3654 (1998).
- ⁶⁰R. H. Swendsen and J.-S. Wang, *Phys. Rev. Lett.* **57**, 2607 (1986).
- ⁶¹A. M. Ferrenberg and R. H. Swendsen, *Phys. Rev. Lett.* **63**, 1195 (1989).
- ⁶²P. L. Privalov and S. A. Potekhin, in *Methods in Enzymology*, Vol. 131 (Academic Press, 1986) pp. 4–51.
- ⁶³Y. Zhou, C. K. Hall, and M. Karplus, *Prot. Sci.* **8**, 1064 (1999).
- ⁶⁴B. Kuhlman, D. L. Luisi, P. A. Evans, and D. P. Raleigh, *J. Mol. Biol.* **284**, 1661 (1998).
- ⁶⁵H. Taskent, J.-H. Cho, and D. P. Raleigh, *J. Mol. Biol.* **378**, 699 (2008).
- ⁶⁶G. Tian, B. E. Shakhnovich, N. V. Dokholyan, and E. I. Shakhnovich, *Proc. Natl. Acad. Sci. USA* **101**, 2846 (2004).
- ⁶⁷P. Faisca and R. Ball, *J. Chem. Phys.* **117**, 8587 (2002).
- ⁶⁸J. D. Bryngelson and P. G. Wolynes, *Proc. Natl. Acad. Sci. USA* **84**, 7524 (1987).
- ⁶⁹H. Nymeyer, A. E. García, and J. N. Onuchic, *Proc. Natl. Acad. Sci. USA* **95**, 5921 (1998).
- ⁷⁰S. S. Plotkin, *Prot. Struct. Func. Bio.* **45**, 337 (2001).
- ⁷¹M. Cieplak and T. X. Hoang, *Int. J. Mod. Phys. C* **13**, 1231 (2002).
- ⁷²D. Sitkoff, K. A. Sharp, and B. Honig, *J. Phys. Chem.* **98**, 1978 (1994).
- ⁷³F. Avbelj, P. Luo, and R. L. Baldwin, *Proc. Natl. Acad. Sci. USA* **97**, 10786 (2000).
- ⁷⁴F. Avbelj and R. L. Baldwin, *Proc. Natl. Acad. Sci. USA* **99**, 1309 (2002).
- ⁷⁵R. L. Baldwin, *J. Bio. Chem.* **278**, 17581 (2003).
- ⁷⁶M. Karplus and D. L. Weaver, *Prot. Sci.* **3**, 650 (1994).
- ⁷⁷M. Doi, *Introduction to Polymer Physics* (Oxford University Press, 1996).
- ⁷⁸P. Ferrara, J. Apostolakis, and A. Cafisch, *Prot. Struct. Func. Bio.* **46**, 24 (2002).
- ⁷⁹B. Lee and F. M. Richards, *J. Mol. Biol.* **55**, 379 (1971).
- ⁸⁰A. G. Street and S. L. Mayo, *Fold. Des.* **3**, 253 (1998).
- ⁸¹Y. Levy and J. N. Onuchic, *Proc. Natl. Acad. Sci. USA* **101**, 3325 (2004).
- ⁸²M. M. Gromiha and S. Selvaraj, *J. Mol. Biol.* **310**, 27 (2001).
- ⁸³D. E. Makarov, C. A. Keller, K. W. Plaxco, and H. Metiu, *Proc. Natl. Acad. Sci. USA* **99**, 3535 (2002).

⁸⁴H. Zhou and Y. Zhou, *Biophys. J.* **82**, 458 (2002).

⁸⁵D. N. Ivankov, S. O. Garbuzynskiy, E. Alm, K. W. Plaxco, D. Baker, and A. V. Finkelstein, *Prot. Sci.* **12**, 2057 (2003).

⁸⁶C. Micheletti, *Prot. Struct. Func. Bio.* **51**, 74 (2003).

⁸⁷H. Gong, D. G. Isom, R. Srinivasan, and G. D. Rose, *J. Mol. Bio.* **327**, 1149 (2003).

⁸⁸P. D. Dixit and T. R. Weikl, *Prot. Struct. Func. Bio.* **64**, 193 (2006).

⁸⁹M. Baiesi, E. Orlandini, F. Seno, and A. Trovato, *J. Phys. A: Math. Gen.* **50**, 504001 (2017).